Available online at www.sciencedirect.com

ScienceDirect

Ceramics International 40 (2014) 6685–6689

CERAMICS INTERNATIONAL

www.elsevier.com/locate/ceramint

V-doped In_2O_3 nanofibers for H_2S detection at low temperature

Juan Liu[a], Wenbin Guo[a], Fengdong Qu[a], Caihui Feng[c], Chao Li[a], Linghui Zhu[a], Jingran Zhou[a,*], Shengping Ruan[b], Weiyou Chen[b,*]

[a]State Key Laboratory on Integrated Optoelectronics, Jilin University, Changchun 130012, PR China
[b]College of Electronic Science and Engineering, Jilin University, Changchun 130012, PR China
[c]College of Instrument Science and Electrical Engineering, Jilin University, Changchun 130012, PR China

Received 25 September 2013; received in revised form 25 November 2013; accepted 26 November 2013
Available online 4 December 2013

Abstract

Pristine and vanadium-doped In_2O_3 nanofibers were fabricated by electrospinning and their sensing properties to H_2S gas were studied. X-ray diffractometry (XRD), X-ray photoelectron spectroscopy (XPS), scanning electron microscopy (SEM) and transmission electron microscopy (TEM) were used to investigate the inner structure and the surface morphology. The H_2S-sensing performances were characterized at different temperatures ranging from 50 to 170 °C. The sensor based on 6 mol% V-doped In_2O_3 nanofibers exhibit the highest response, i.e. 13.9–50 ppm H_2S at the relatively low temperature of 90 °C. In addition, the fast response (15 s) and recovery (18 s) time, and good selectivity were observed.

Keywords: E. Sensor; Electrospinning; V-doped In_2O_3; Nanofibers; H_2S

1. Introduction

The air pollution is a global problem, especially H_2S, a bad smelling and toxic gas, which harms our health very much. So it is of great interest to develop a reliable and effective H_2S gas sensor [1,2]. A large number of H_2S detecting systems have currently been used [3]. Among them, gas sensors based on metal oxides attract great attention due to their low cost, production flexibility, convenient use and detectable possibility of large number of gases [4,5].

As we know, the sensing response of oxide films is highly dependent on their surface structure and morphology [6]. In order to get better performance gas sensors with high sensitivity, high selectivity and rapid response rate, one-dimensional (1D) nanostructure metal oxide semiconductor (MOS) with large specific surface such as nanofibers, nanowires, nanotubes, nanobelts, etc., has received much interest [7]. There are a lot of methods to synthesize 1D nanomaterials such as template-assisted sol–gel [8], chemical vapor deposition (CVD) [9], electrospinning [10], hydrothermal [11], etc. Electrospinning is recognized as a simple and versatile method to synthesize various fiber assemblies [7], which can enhance the performance of products made from nanofibers and allow to apply specific modifications [12].

Indium oxide (In_2O_3) is an n-type semiconductor with a bandgap of 3.55–3.75 eV [13] and has been widely used in UV lasers [14], gas sensors [15], solar cells [16,17], flat-panel displays [18] due to its excellent optical transparency for visible light and high electrical conductivity [16]. Pure In_2O_3 has been intensively attempted to detect gas for a long time. However, there are still some disadvantages that need to be overcome to satisfy the practical requirements. Recently, two kinds of studies, associated with further enhanced response parameters, have attracted much interest: one is increasing the surface area to get a higher surface to volume ratio to promote the surface-controlled process between target gas and In_2O_3 sensor and the other is decorating In_2O_3 surface with noble metals (like Au, Ag, Pt, Cu) [19–22] or doping In_2O_3 with metals (Ni, Sn, Ti) [13,23,24] to improve the catalytic activity.

In this paper, we attempted to fabricate vanadium doped In_2O_3 solid solution by electrospinning combined with a

*Corresponding authors. Tel.: +86 431 85168240x8219; fax: +86 431 85168270.
E-mail addresses: zhoujjr1989@gmail.com (J. Zhou), bjuqingqing@gmail.com (W. Chen).

0272-8842/$ - see front matter © 2013 Elsevier Ltd and Techna Group S.r.l. All rights reserved.
http://dx.doi.org/10.1016/j.ceramint.2013.11.129

calcination process. The hydrogen sulfide sensing properties were investigated. The sensor based on 6 mol% V-doped In_2O_3 can detect H_2S efficiently at the relatively low temperature of 90 °C which indicates that the fabricated nanomaterial is a better candidate for H_2S detection.

2. Experimental

2.1. Chemical reagents

All the used materials for the synthesization of V-doped In_2O_3 nanofibers are (AR grade): $In(NO_3)_3 \cdot 4.5H_2O$, C_2H_5OH, *N,N*-dimethylformamide (DMF), vanadium triisopropoxy oxide ($C_9H_{21}O_4V$) and polyvinyl pyrrolidone (PVP, $M_w \approx 1{,}300{,}000$) were purchased from Aladdin Chemistry Co. Ltd.

2.2. Preparation of pristine and V-doped In_2O_3 nanofibers

To synthesis pristine and V-doped In_2O_3 nanofibers, 8.8 g ethanol and *N,N*-dimethylformamide (DMF) were mixed together at a weight ratio of 1:1. Then, 0.4 g $In(NO_3)_3 \cdot 4.5H_2O$ and a suitable amount of vanadium triisopropoxy oxide ($C_9H_{21}O_4V$) were added into the above solvent. After being stirred for 2 h, 0.8 g PVP was added to it. After being further stirred for 6 h, the obtained solution was then transferred into a plastic syringe with a metal needle which was connected to a high-voltage power supply. A voltage of 20 kV was applied between the cathode (a flat aluminum foil) and the anode (syringe tip) at a distance of 20 cm. The $In(NO_3)_3$/PVP composite nanofibers were obtained on the foil. Then the composite nanofibers were transferred into a muffle and calcined at 600 °C for 4 h in air to remove organic constituents and convert the precursor into crystal nanofibers.

3. Characterization

The prepared nanofibers were characterized by X-ray diffractometry (XRD) (Shimadzu XRD-6000, Cu-Kα radiation); X-ray photoelectron spectroscopy (XPS) (VG ESCA LAB MKII, Mg Kα radiation); scanning electron microscopy (SEM) (XL30E-SEMFEG) and transmission electron microscopy (TEM) (JEM-ARM200F).

4. Sensor fabrication and measurement

The fabrication process of gas sensor is as follows: the as-synthesized sample (pure and V-doped In_2O_3 nanofibers) was mixed with deionized water at a weight ratio of 100:25 to form a paste. The paste was then coated on a ceramic tube, on which a pair of Au electrodes was already printed to form a sensing film with a thickness of about 300 μm. Pt leading wires attached to the electrodes were used as electrical contacts. After the ceramic tube was calcined at 300 °C for 2 h, a Ni–Cr heating wire was inserted into the tube as a heater to control the operating temperature.

The fabricated sensor was measured by a CGS-8 (Chemical gas sensor-8) intelligent gas sensing analysis system (Beijing Elite Tech Co., Ltd., China). Firstly, we mixed the target gas (H_2S) with air in a glass test chamber. Then put the sensor into the glass chamber. When the sensitivity achieved a stable value, the device was taken out to recover in air.

The response (S) was measured from 55 to 160 °C by comparing the resistance of the sensor in air (R_a) with that in target gases (R_g). The cost time of the sensor achieving 90% of the total resistance is defined as the response time in the case of adsorption or the recovery time in the case of desorption [25].

5. Results and discussion

5.1. Nanofiber characterization

Fig. 1 shows the XRD patterns of the pure In_2O_3 and $In_{2-x}V_xO_3$ nanofibers with different molar ratios (4 mol%, 6 mol%, and 8 mol%) of vanadium. It can be observed that all the diffraction peaks correspond to the cubic indium oxide (JCPDS card no. 06-0416) [13]. For the V-doped nanofibers, no impure phases corresponding to vanadium compounds were detected, which indicated that the V element is effectively incorporated into the In_2O_3 crystal lattice to form a stable $In_{2-x}V_xO_3$ substitution solid solution. However, compared with the pure In_2O_3, the intensity of V-doped In_2O_3 diffraction peaks decrease sharply, indicating that the crystallization of V-doped In_2O_3 becomes weak, which suggests that a certain amount of V demotes the crystallization of In_2O_3 [26]. The average sizes of pure In_2O_3, 4 mol%, 6 mol%, and 8 mol% V-doped In_2O_3 crystallite were calculated to be ~20.8, 11.4, 11.0 and 14.0 nm respectively according to Scherrer's equation. The peaks of V-doped In_2O_3 nanofibers were slightly shifted to a higher 2θ value compared with those of pure In_2O_3 nanofibers, which is attributed to the decreased lattice spacings due to smaller V^{5+} (0.580 Å) ions [27] in place of In^{3+} (0.800 Å) [28]. The lattice parameters *a* calculated from the XRD measurements of pure In_2O_3, 4 mol%, 6 mol%, and 8 mol% V-doped In_2O_3 crystallite are 10.136, 10.117, 10.109, 10.057 Å, respectively.

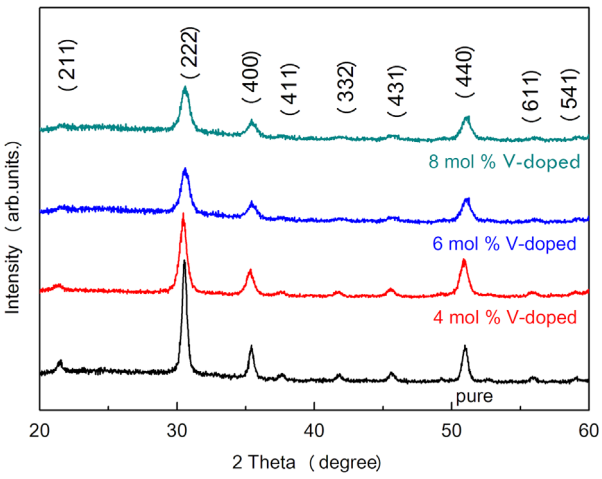

Fig. 1. XRD patterns of pure and V-doped In_2O_3 nanofibers.

The 6 mol% V-doped In_2O_3 nanofibers were also studied by XPS analysis, which is shown in Fig. 2. The four peaks with binding energies 515.9, 517.3, 522.8, and 524.6 eV correspond to V^{3+} $2p_{3/2}$, V^{5+} $2p_{3/2}$, V^{3+} $2p_{1/2}$ and V^{5+} $2p_{1/2}$ respectively, which further indicates the formation of $In_{2-x}V_xO_3$ solid solution [27].

The SEM images of electrospun composite nanofibers before and after calcination are shown in Fig. 3(a)–(d). It can be seen that the $In(NO_3)_3$/PVP composite (a) and In $(NO_3)_3$/PVP/$C_9H_{21}O_4V$ composite nanofibers (c) with smooth and uniform surface were collected as randomly oriented structures in the form of nonwoven mats [13]. The average diameters are approximately 400 nm (pure In_2O_3) and 267 nm (6 mol% V-doped In_2O_3). After calcination at 600 °C, the nanofibers shrank and became bent and rough, but still maintained the continuous structure. The average diameters decreased to 117 nm (In_2O_3) and 95 nm (6 mol% V-doped In_2O_3). Further morphology characterization of the 6 mol% V-doped In_2O_3 nanofibers was examined by TEM (Fig. 3(e)), which agreed with SEM results properly. The SAED pattern shown in Fig. 3(f) indicates that the 6 mol% V-doped In_2O_3 nanofibers are polycrystalline in structure.

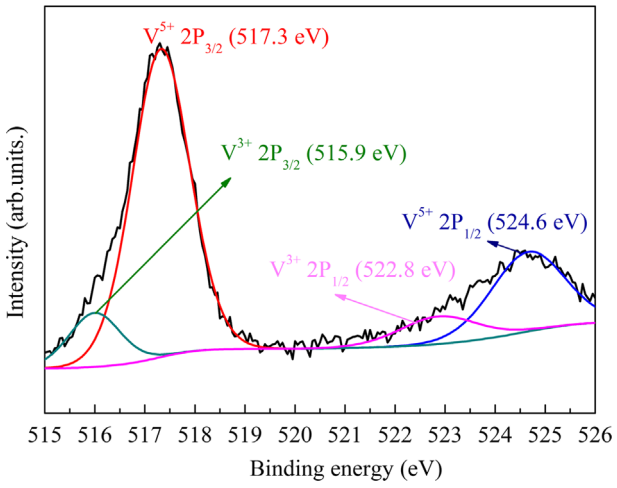

Fig. 2. XPS spectrum of 6 mol% V-doped In_2O_3 nanofibers.

5.2. Evaluation of gas-sensing performance

Fig. 4 shows the response as a function of operating temperature from 55 to 160 °C for the pristine In_2O_3 and $In_{2-x}V_xO_3$ (4 mol%, 6 mol% and 8 mol%) exposed to 50 ppm hydrogen sulfide (H_2S). In the range of the operating temperatures, the response values increase sharply at the beginning and then decrease dramatically. The maximum response value of each sensor arrived at a certain temperature (pure and 4 mol%: 85 °C, 6 mol% and 8 mol%: 90 °C). Moreover, the 6 mol% V-doped In_2O_3 exhibits a higher sensitivity than the other

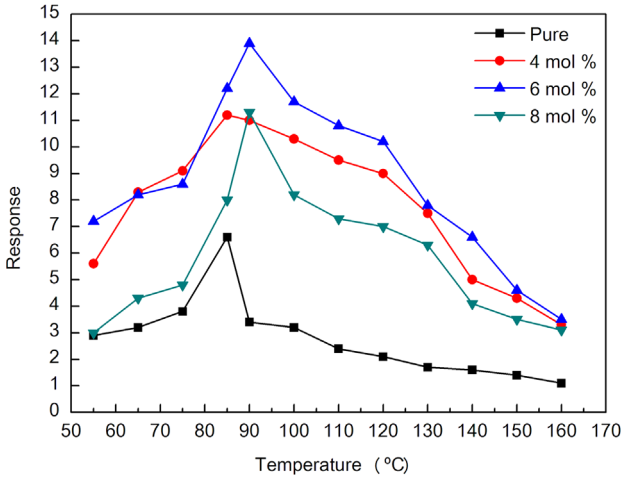

Fig. 4. Responses of pure and 6 mol% V-doped In_2O_3 nanofibers to 50 ppm H_2S at different operating temperatures.

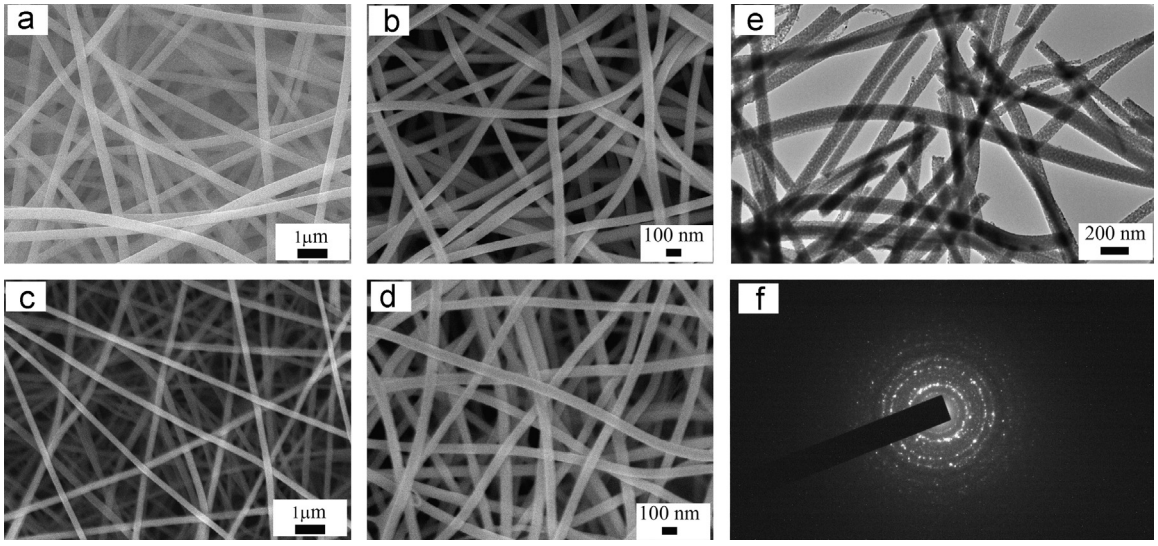

Fig. 3. SEM images of $In(NO_3)_3$/PVP composite nanofibers (a); $In(NO_3)_3$/PVP/$C_9H_{21}O_4V$ composite nanofibers (c); In_2O_3 nanofibers (b); and 6 mol% V-doped In_2O_3 nanofibers (d). The TEM images (e) of 6 mol% V-doped nanofibers In_2O_3 and SAED pattern (f).

sensors, which shows that 6 mol% is the optimum doping concentration.

The response and recovery characteristics of pristine and 6 mol% V-doped In_2O_3 to 50 ppm H_2S at their own optimum working temperature are shown in Fig. 5. It can be seen that the response and recovery rate of 6 mol% V-doped In_2O_3 nanofiber is much higher than that of the pure nanofibers. Moreover, when the target gas was injected into the testing chamber, the responses of both sensors increased rapidly; when subjected to air, the sensor recovered to initial state rapidly. The rapid response and recovery of the sensor can be attributed to the 1D nanostructure of the as-electrospun nanofibers, which can facilitate fast mass transfer of H_2S molecules to the interaction region and improve the rate for the charge carriers to traverse the barriers introduced by molecular recognition events along the entire fibers [29,30].

In the following investigation, the sensitivities of pristine and 6 mol% V-doped In_2O_3 sensors versus H_2S concentration were observed at 85 °C and 90 °C. The results are shown in Fig. 6. It can be seen that the sensitivity of each one increases with the increasing H_2S concentration at the beginning, and then tends to be saturated when the concentration is higher than 500 ppm. Also in the whole detecting range, the 6 mol% V-doped In_2O_3 nanofibers exhibit much higher sensitivity than pristine In_2O_3 nanofibers resulting in the 6 mol% V-doped In_2O_3 possessing a better sensitive property to H_2S.

Finally, sensing selectivity of 6 mol% V-doped In_2O_3 nanofibers was investigated to evaluate the sensing property. The cross responses of 6 mol% V-doped In_2O_3 nanofibers to 50 ppm different gases such as HCHO, H_2, CO, NO_2, CH_4, C_8H_{10}, NH_3, C_2H_5OH, and H_2S at 90 °C are shown in Fig. 7. As can be seen, the sensor exhibits much higher response to H_2S than other gases. The observed high sensitivity and selectivity of the 6 mol% V-doped In_2O_3 nanofibers shows that it is a suitable candidate for monitoring low concentrations of H_2S.

The sensing mechanism can be explained as follows: the resistance change of $In_{2-x}V_xO_3$ gas sensors is primarily caused by the adsorption and desorption of H_2S molecules

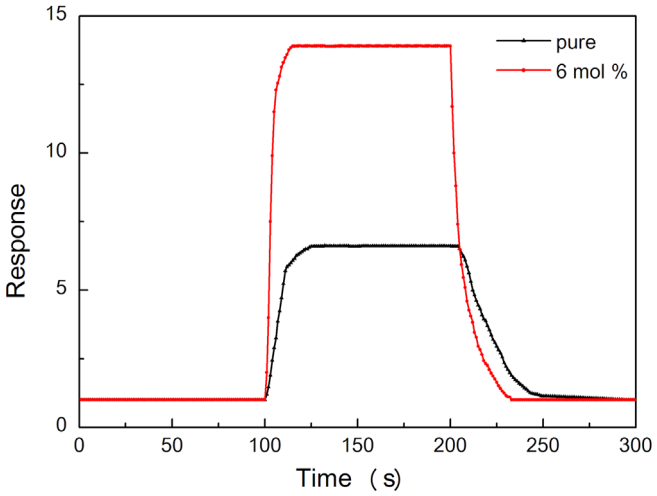

Fig. 5. The response and recovery characteristics of pure and 6 mol% V-doped In_2O_3 to 50 ppm H_2S at 85 °C and 90 °C respectively.

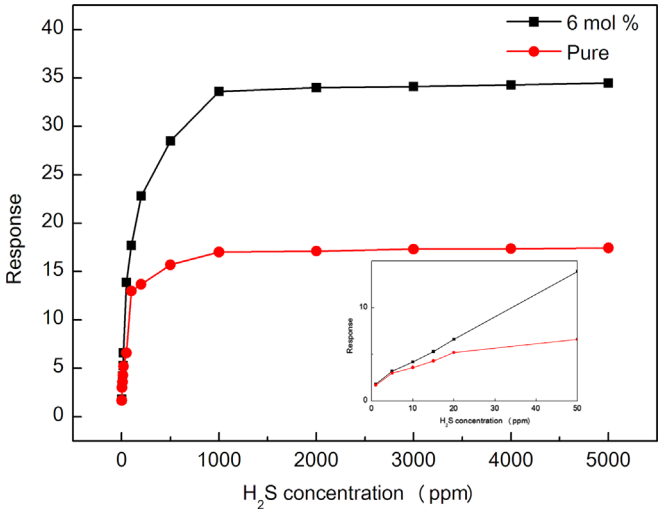

Fig. 6. The response of the pure and the 6 mol% V-doped In_2O_3 nanofibers versus H_2S concentrations; the inset is the calibration curve in the range of 1–500 ppm.

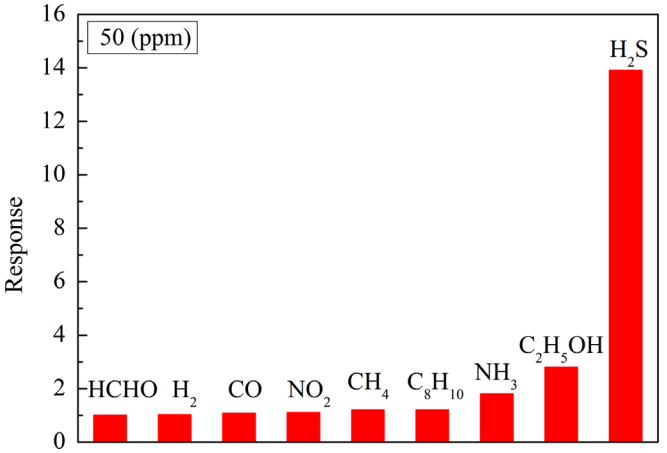

Fig. 7. Responses of 6 mol% V-doped In_2O_3 nanofibers to different gases at 90 °C.

on the surface of $In_{2-x}V_xO_3$ film [31,32]. When $In_{2-x}V_xO_3$ nanofibers are exposed to air, oxygen is adsorbed on the exposed surface of $In_{2-x}V_xO_3$ and ionized to O^- or O^{2-}, resulting in a decrease in carrier concentration and electron mobility. When exposed to the reducing concentration of H_2S, H_2S will react with the adsorbed oxygen molecules and release the trapped electrons back to the conduction band, which increases the carrier concentration and carrier mobility of $In_{2-x}V_xO_3$. Therefore the resistance change of the $In_{2-x}V_xO_3$ can easily be observed. The process of the reaction can be described as follows:

$$O_2\ (\text{gas}) + 2n\ e^- \leftrightharpoons 2O^{n-}\ (\text{ads})\ (n=1 \text{ or } 2) \quad (1)$$

$$H_2S\ (\text{gas}) + 3O^{n-}\ (\text{ads}) \leftrightharpoons H_2O\ (\text{gas}) + SO_2\ (\text{gas}) + 3n\ e^- \quad (2)$$

The high sensitivity and quick response of the current nanofibers are attributed to their 1D nanostructure with high surface-to-volume ratio, which drives the sensor device to

absorb more H_2S molecules and form web-like structure on the sensor surface naturally. Simultaneously, the solid solution system can produce more vacant oxygen, leading more oxygen species being absorbed on the surface of $In_{2-x}V_xO_3$ solid solution nanofibers, which eventually improves the sensing performances of the device.

6. Conclusions

In summary, pure In_2O_3 and solid state solution $In_{2-x}V_xO_3$ nanofibers with different V-dopings were synthesized through electrospinning method and their sensing properties of H_2S were investigated. The results showed that V-doping can reduce the diameters of In_2O_3 fibers and improve their sensing performance of H_2S greatly. $In_{2-x}V_xO_3$ sensor with 6 mol% V-doping exhibits the highest response and best selectivity among all the samples.

Acknowledgments

The authors are grateful to National Natural Science Foundation of China (Grant nos. 61006013, 61007022, 61275035, 61274068, and 61077046), Chinese National Programs for High Technology Research and Development (Grant no. 2013AA030902), Doctoral Found of Ministry of Education of China (Grant nos. 20100061120045, and 20110061130004), Project of Science and Technology Development Plan of Jilin Province (Grant nos. 20130206075SF, and 20110314, 20120324), Scientific Frontier and Interdiscipline Innovative Projects of Jilin University (Grant no. 2013ZY18), the Opened Fund of the State Key Laboratory on Integrated Optoelectronics (No. IOSKL2012KF03) for the support to the work.

References

[1] I.A. Yang, S.T. Holgate, Air pollution and lung health: an epilogue, Respirology 18 (2013) 3–4.
[2] J. Liu, X. Huang, G. Ye, W. Liu, Z. Jiao, W. Chao, Z. Zhou, Z. Yu, H_2S detection sensing characteristic of CuO/SnO_2 sensor, Sensors 3 (2003) 110–118.
[3] G.N. Advani, L. Nanis, Effects of humidity on hydrogen sulfide detection by SnO_2 solid state gas sensors, Sens. Actuators 2 (1981) 201–206.
[4] N. Barsan, D. Koziej, U. Weimar, Metal oxide-based gas sensor research: how to?, Sens Actuators, B 121 (2007) 18–35.
[5] C. Matei Ghimbeu, J. Schoonman, M. Lumbreras, Porous indium oxide thin films deposited by electrostatic spray deposition technique, Ceram. Int. 34 (2008) 95–100.
[6] Y. Qin, G. Fan, K. Liu, M. Hu, Vanadium pentoxide hierarchical structure networks for high performance ethanol gas sensor with dual working temperature characteristic, Sens. Actuators, B 190 (2014) 141–148.
[7] P. Rai, Y.-S. Kim, H.-M. Song, M.-K. Song, Y.-T. Yu, The role of gold catalyst on the sensing behavior of ZnO nanorods for CO and NO_2 gases, Sens. Actuators, B 165 (2012) 133–142.
[8] B.B. Lakshmi, P.K. Dorhout, C.R. Martin, Sol – Gel template synthesis of semiconductor nanostructures, Chem. Mater. 9 (1997) 857–862.
[9] G. Che, B.B. Lakshmi, C.R. Martin, E.R. Fisher, R.S. Ruoff, Chemical vapor deposition based synthesis of carbon nanotubes and nanofibers using a template method, Chem. Mater. 10 (1998) 260–267.
[10] Z.-M. Huang, Y.Z. Zhang, M. Kotaki, S. Ramakrishna, A review on polymer nanofibers by electrospinning and their applications in nano-composites, Compos. Sci. Technol. 63 (2003) 2223–2253.
[11] W.N. Li, J. Yuan, X.F. Shen, S. Gomez-Mower, L.P. Xu, S. Sithambaram, M. Aindow, S.L. Suib, Hydrothermal synthesis of structure- and shape-controlled manganese oxide octahedral molecular sieve nanomaterials, Adv. Funct. Mater. 16 (2006) 1247–1253.
[12] W.E. Teo, S. Ramakrishna, A review on electrospinning design and nanofibre assemblies, Nanotechnology 17 (2006) R89.
[13] C. Feng, W. Li, C. Li, L. Zhu, H. Zhang, Y. Zhang, S. Ruan, W. Chen, L. Yu, Highly efficient rapid ethanol sensing based on $In_{2-x}Ni_xO_3$ nanofibers, Sens. Actuators, B 166–167 (2012) 83–88.
[14] H. Imai, A. Tominaga, H. Hirashima, M. Toki, M. Aizawa, Ultraviolet-laser-induced crystallization of sol–gel derived indium oxide films, J. Sol–Gel Sci. Technol. 13 (1998) 991–994.
[15] X. Zou, J. Wang, X. Liu, C. Wang, Y. Jiang, Y. Wang, X. Xiao, J.C. Ho, J. Li, C. Jiang, Y. Fang, W. Liu, L. Liao, Rational design of sub-parts per million specific gas sensors array based on metal nanoparticles decorated nanowire enhancement-mode transistors, Nano Lett. 13 (2013) 3287–3292.
[16] P. Qin, G. Fang, N. Sun, X. Fan, Q. Zheng, F. Cheng, J. Wan, X. Zhao, P-type indium oxide thin film for the hole-transporting layer of organic solar cells, Thin Solid Films 520 (2012) 3118–3124.
[17] T.-T. Tseng, W.J. Tseng, Effect of polyvinylpyrrolidone on morphology and structure of In_2O_3 nanorods by hydrothermal synthesis, Ceram. Int. 35 (2009) 2837–2844.
[18] B.H. Lee, K. Iee Gon, C. Sung Woo, S.-H. Lee, Effect of process parameters on the characteristics of indium tin oxide thin film for flat panel display application, Thin Solid Films 302 (1997) 25–30.
[19] L.H. Qian, K. Wang, Y. Li, H.T. Fang, Q.H. Lu, X.L. Ma, CO sensor based on Au-decorated SnO_2 nanobelt, Mater. Chem. Phys. 100 (2006) 82–84.
[20] E.H. Espinosa, R. Ionescu, C. Bittencourt, A. Felten, R. Erni, G. Van Tendeloo, J.J. Pireaux, E. Llobet, Metal-decorated multi-wall carbon nanotubes for low temperature gas sensing, Thin Solid Films 515 (2007) 8322–8327.
[21] A. Kaniyoor, R. Imran Jafri, T. Arockiadoss, S. Ramaprabhu, Nanos-tructured Pt decorated graphene and multi walled carbon nanotube based room temperature hydrogen gas sensor, Nanoscale 1 (3) (2009) 382.
[22] J. Luo, S. Jiang, H. Zhang, J. Jiang, X. Liu, A novel non-enzymatic glucose sensor based on Cu nanoparticle modified graphene sheets electrode, Anal. Chim. Acta 709 (2012) 47–53.
[23] A. Okamoto, I. Shibasaki, Transport properties of Sn-doped InSb thin films and applications to Hall element, J. Cryst. Growth 251 (2003) 560–564.
[24] L.G. Bloor, J. Manzi, R. Binions, I.P. Parkin, D. Pugh, A. Afonja, C.S. Blackman, S. Sathasivam, C.J. Carmalt, Tantalum and titanium doped In_2O_3 thin films by aerosol-assisted chemical vapor deposition and their gas sensing properties, Chem. Mater. 24 (2012) 2864–2871.
[25] Y. Hu, O.K. Tan, W. Cao, W. Zhu, A low temperature nano-structured $SrTiO_3$ thick film oxygen gas sensor, Ceram. Int. 30 (2004) 1819–1822.
[26] Y. Zhang, Z. Zheng, F. Yang, Highly sensitive and selective alcohol sensors based on Ag-doped In_2O_3 coating, Ind. Eng. Chem. Res. 49 (2010) 3539–3543.
[27] Y. Wu, C. Nguyen, S. Seraji, M.J. Forbess, S.J. Limmer, T. Chou, G. Cao, Processing and properties of strontium bismuth vanadate niobate ferroelectric ceramics, J. Am. Ceram. Soc. 84 (2001) 2882–2888.
[28] A. Singhal, S.N. Achary, J. Manjanna, O.D. Jayakumar, R.M. Kadam, A.K. Tyagi, Colloidal Fe-doped indium oxide nanoparticles: facile synthesis, structural, and magnetic properties, J. Phys. Chem. C 113 (2009) 3600–3606.
[29] W. Wang, H. Huang, Z. Li, H. Zhang, Y. Wang, W. Zheng, C. Wang, Zinc oxide nanofiber gas sensors via electrospinning, J. Am. Ceram. Soc. 91 (2008) 3817–3819.
[30] Y.J. Chen, X.Y. Xue, Y.G. Wang, T.H. Wang, Synthesis and ethanol sensing characteristics of single crystalline SnO_2 nanorods, Appl. Phys. Lett. 87 (2005) 233503–233503-3.
[31] X. Wang, M. Zhang, J. Liu, T. Luo, Y. Qian, Shape- and phase-controlled synthesis of In_2O_3 with various morphologies and their gas-sensing properties, Sens. Actuators, B 137 (2009) 103–110.
[32] J.-X. Wang, L.-X. Yu, H.-M. Wang, S.-P. Ruan, J.-J. Li, F.-Q. Wu, Preparation and triethylamine sensing properties of Ce-doped In_2O_3 nanofibers, Acta Phys.-Chim. Sin. 26 (2010) 3101–3105.